

Flavor Degeneracy and Effects of Disorder in Ultracold Atom Systems

Walter Hofstetter

Institut fuer Theoretische Physik A, RWTH Aachen, Templergraben 55,
52056 Aachen, Germany

Abstract. Cold atoms in optical lattices offer an exciting new laboratory where quantum many-body phenomena can be realized in a highly controlled way. They can serve as *quantum simulators* for notoriously difficult problems like high-temperature superconductivity. This review is focussed on recent developments and new results in multi-component systems. Fermionic atoms with $SU(N)$ symmetry have exotic superfluid and flavor-ordered ground states. We discuss symmetry breaking, collective modes and detection issues. Bosonic multi-flavor ensembles allow for engineering of spin Hamiltonians which are interesting from a quantum computation point of view. Finally, we will address the competition of disorder and interaction in optical lattices. We present a complete phase diagram obtained within dynamical mean-field theory and discuss experimental observability of the Mott and Anderson phases.

1 Introduction and Overview

The achievement of Bose-Einstein condensation (BEC) 10 years ago [1] has opened the new field of interacting quantum gases in the dilute limit. It has become possible to observe quantum phenomena like Bose statistics on a mesoscopic scale, involving a large number of atoms. More recently, fermionic gases have also been cooled to the quantum degenerate regime, using sympathetic cooling of two spin states or boson-fermion mixtures [2,3,4,5]. Although the resulting temperatures $T/T_F \approx 0.1$ are, relatively to the Fermi temperature T_F , much higher than in solids, the Pauli principle has been clearly observed.

In addition to quantum statistics, tunable interactions are another important ingredient in the cold atom "toolbox". The interactions between atoms can be changed by an external magnetic field as a result of Feshbach resonances [6,7]. In particular, their scattering length can be tuned to positive or negative values, corresponding to repulsive or attractive interactions. This has opened the way to studies of solid-state related phenomena like Cooper pairing and BCS superfluidity of fermions [8,9]. The resulting BEC-BCS crossover has recently been the subject of intense experimental and theoretical studies [10,11,12]

In an independent development, degenerate atomic clouds have been combined with optical lattices, created by standing light waves which generate an effective periodic potential for the atoms [13,14,15]. Interactions can

thus be tuned without changing the atomic scattering length. This has been demonstrated in a pathbreaking experiment [14] where interacting bosons were tuned through a quantum phase transition from a superfluid (SF) to a Mott insulating state. Very recently, fermionic K^{40} atoms have been loaded into 3d optical lattices as well [16]. In these new experiments the lowest Bloch band was filled up successively, and the shape of the Fermi surface monitored by time-of-flight measurements. Eventually a completely filled Brillouin zone corresponding to a band insulator was observed.

More generally, fermionic atoms in optical lattices allow for the realization of solid-state type quantum phases like antiferromagnetism or high-temperature superconductivity [17]. Even the spatial dimensionality of the lattice can be tuned. As an example, one-dimensional optical lattices have been realized where the hardcore or Tonks-gas limit of interacting bosons has been observed [18,19,20]. Recent progress in numerical methods for simulating 1d quantum systems has led to interesting predictions about the dynamics of such systems [21,22].

In the following we will first introduce the basic model describing cold atoms in optical lattices. We will then address systems with multiple flavors, i.e. hyperfine states, which allow realization of new exotic quantum states not accessible in solids. Finally, we will discuss the role of disorder in current and future experiments involving cold atoms.

2 Optical Lattices and Strong Correlations

2.1 Model and Parameters

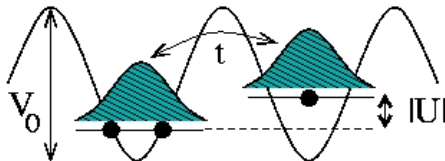


Fig. 1. Cold atoms in an optical lattice of strength V_0 , shown here with hopping t and negative onsite interaction U . This situation corresponds to an attractive Hubbard model where multiple occupancy of lattice sites is energetically favourable.

Atoms can be trapped in standing light waves created by interfering laser beams detuned far from resonance [13,14,15]. Due to the AC Stark shift the atoms experience a periodic potential of the form $V(x) = V_0 \sum_{i=1,2,3} \cos^2(kx_i)$ where k is the wave vector of the laser. The natural energy scale for the potential depth V_0 is the recoil energy $E_R = \hbar^2 k^2 / 2m$. A schematic picture of such an optical lattice is shown in Fig. 1. The eigenstates in the periodic

lattice potential are given by Bloch bands, and an equivalent representation in terms of Wannier orbitals leads to a tight-binding Hamiltonian. Let us assume for the moment that two different (hyperfine-) spin states are present, which in the following are denoted as $\sigma = \uparrow, \downarrow$. If temperature and filling are sufficiently low, the atoms will be confined exclusively to the lowest Bloch band. In this case the system can be described by a Hubbard Hamiltonian [23,15]

$$H = -t \sum_{\langle ij \rangle, \sigma} (c_{i\sigma}^\dagger c_{j\sigma} + c_{j\sigma}^\dagger c_{i\sigma}) + U \sum_i n_{i\uparrow} n_{i\downarrow} \quad (1)$$

where $\langle ij \rangle$ labels next neighbors, $c_{i\sigma}$ is the fermionic annihilation operator for the Wannier state of spin σ on site i and $n_{i\sigma} = c_{i\sigma}^\dagger c_{i\sigma}$ is the corresponding number density. The parameters for hopping and onsite interaction can then be expressed as $t = E_R(2/\sqrt{\pi})\xi^3 \exp(-2\xi^2)$ and $U = E_R a_s k \sqrt{8/\pi} \xi^3$. Here a_s is the atomic scattering length and $\xi = (V_0/E_R)^{1/4}$ is a parameter characterizing the strength of the lattice [15,17]. It is obvious that by tuning the optical lattice potential V_0 one can achieve arbitrary ratios $|U|/t$ without changing a_s . Optical lattices thus give access to the *strongly correlated* regime without using Feshbach resonances.

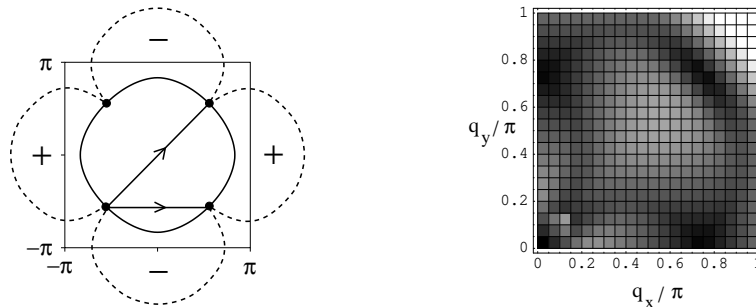


Fig. 2. Probing d -wave pairing in the repulsive 2d Hubbard model via Bragg scattering. Left: schematic diagram of the Fermi surface in 2d (solid line) and the momentum dependence of the gap (dashed line). Right: onset frequency of the quasiparticle continuum in the dynamical structure factor $S(q, \omega)$, plotted as a function of momentum q . At the special wave vectors connecting the nodal points in the left figure, the density response is gapless. Figures taken from [17].

2.2 Quantum Simulations

The Hubbard model (1) is of fundamental importance for electronic correlation effects in condensed matter. From this point of view, ultracold atoms can be used to perform *quantum simulations* of solid state physics. Here we

illustrate this intriguing idea with the example of high-temperature d-wave superconductivity [17].

Consider the 2d Hubbard Hamiltonian (1) with spin-1/2 fermions and repulsive interaction $U > 0$ resulting from a positive scattering length $a_s > 0$. At half filling $n_i = 1$ this model gives rise to staggered antiferromagnetic order. At lower filling fractions, theoretical arguments suggest a d-wave paired phase, which is a possible candidate for explaining high-temperature superconductivity in the cuprates [24]. However, there is no satisfactory numerical evidence, mainly because quantum Monte Carlo calculations are limited to extremely small systems due to the sign problem.

On the other hand, cold fermions in an optical lattice could be used to *experimentally* probe d-wave pairing in the 2d Hubbard model. The resulting superfluid order can be detected via Bragg scattering, as shown in Fig. 2, which is by now a well-established technique to measure the dynamical density response $S(q, \omega)$ in interacting quantum gases [25]. As already suggested by Feynman [26], such quantum simulations could provide a powerful tool to gain insight into many-body Hamiltonians relevant for solid-state physics.

3 Multi-Component Systems

3.1 Two-Component Bosons with Spin Order

All of the alkali atoms available for trapping and cooling have $2 * (2I + 1)$ low-lying hyperfine states, where I is the nuclear spin. Several of these states can be trapped at the same time: in magnetic traps one is limited by the condition that the states have to be *low-field seekers*, but optical dipole traps, as well as optical lattices, allow confinement of basically any combination of spin states [27], as long as no instability due to three-body collision occurs. Loading a lattice with two hyperfine states of Rb⁸⁷ has been demonstrated experimentally in [28] where also a spin-dependent periodic potential has been implemented. In the following we discuss a proposal, described in detail in [29], how these techniques can be used to engineer quantum spin Hamiltonians which in turn could be relevant for quantum information processing.

Let us consider a system of two bosonic hyperfine states in a lattice, described by the following Bose-Hubbard Hamiltonian:

$$\begin{aligned}
 H = & -t_a \sum_{\langle ij \rangle} (a_i^\dagger a_j + H.c) - t_b \sum_{\langle ij \rangle} (b_i^\dagger b_j + H.c) + U \sum_i (n_{ai} - \frac{1}{2})(n_{bi} - \frac{1}{2}) \\
 & + \frac{1}{2} \sum_{i, \alpha=a,b} V_\alpha n_{\alpha i} (n_{\alpha i} - 1) - \sum_{i, \alpha} \mu_\alpha n_{\alpha i}.
 \end{aligned} \tag{2}$$

Here a_i, b_i denote the annihilation operators for two different bosonic pseudospin states, and the number operators are defined as $n_{ai} = a_i^\dagger a_i$, $n_{bi} = b_i^\dagger b_i$, with the corresponding chemical potentials $\mu_{a(b)}$. In reality, experiments are

performed at a fixed numbers of particles, which in the grand canonical description can be achieved by tuning the chemical potential. The onsite interaction between equal spin states is given by $V_{a(b)}$, and the one between different spins by U . We also assume a spin dependent tunable hopping $t_{a(b)}$ which has already been experimentally realized [28].

We now focus on the case of integer filling $n_a + n_b = 1$, following [29]. We are mainly interested in the nature of the Mott-superfluid transition in this system, and the possibility of spin order in the insulating phase. To address the second issue, it is instructive to first consider parameters $t_{a,b} \ll U, V_{a,b}$ deep inside the Mott phase. States with double occupancy per site are then very unfavourable and can be projected out by a Schrieffer-Wolff transformation. This leads to an effective spin Hamiltonian in the subspace of single occupation [30]. The physics of this XXZ model is well understood and includes an x-y ferromagnetic phase as well as an antiferromagnetic z-Neel ordered state.

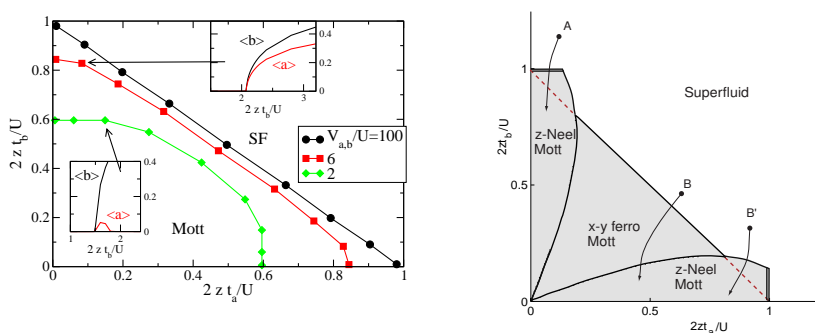


Fig. 3. Left: Phase diagram of the 2-component bosonic Hubbard model obtained by mean-field theory. Note that as $V_{a(b)}$ decreases, the Mott domain shrinks. Right: Phase diagram including quantum fluctuations. Figures taken from [29].

The disadvantage of this deep Mott regime is that the critical temperature for magnetic ordering is very low $T_c \sim \max(t_{a(b)}^2/U, t_{a(b)}^2/V_{a(b)})$ and therefore experimentally hardly accessible. In order to enhance T_c and study the region close to the Mott-SF transition is necessary to make at least one of the interaction parameters comparable to the hopping. Here we choose $t_{a(b)} \approx U \ll V_{a(b)}$, which means that double occupancy with two different spins is now possible. The main question is whether the spin order discussed above is still visible close to the superfluid. In order to map out the Mott-SF phase boundary, we have used a mean-field approach first proposed in [31], where the kinetic energy is decoupled.

The phase diagram obtained in this way is shown in Fig. 3 (left). Note that as $V_{a(b)}$ decreases, the Mott domain shrinks. In order to resolve different spin states in the insulator, it is necessary to take into account quantum fluctuations on top of the variational mean-field state and compare the resulting ground state energies. Details of this calculation can be found in [29]. The resulting phase diagram including fluctuations is shown in Fig. 3 (right). Spin ordering persists right up to the SF phase boundary and can be tuned from xy-ferromagnetic to z-Neel antiferromagnetic by the ratio t_a/t_b . We find hysteresis between the Neel state and the superfluid, while the transition between the xy-state and the SF is continuous. These should be clear signatures for an experimental detection of spin ordered states, using for example Rb⁸⁷ atoms. The spin order can be directly observed by spin-dependent Bragg scattering or via density fluctuations in time-of-flight measurements [32].

3.2 Beyond Solid-State: SU(N) Fermions

We will now show that with the degrees of freedom offered by ultracold atoms it is possible to create new states of matter that have no equivalent in condensed matter. The obvious constraint in solid-state physics is that electrons have only two spin states. Atoms, on the other hand, have large hyperfine multiplets out of which several states can be trapped simultaneously. For fermionic atoms this has been demonstrated with the three states $|F = 9/2, m_F = -5/2, -7/2, -9/2\rangle$ of K⁴⁰ in an optical trap [33]. Alternatively, one could use the three spin polarized $m_s = 1/2$ states of Li⁶ which, in a sufficiently large field, have a pairwise equal and anomalously large triplet scattering length $a_s = -2160a_0$ [34].

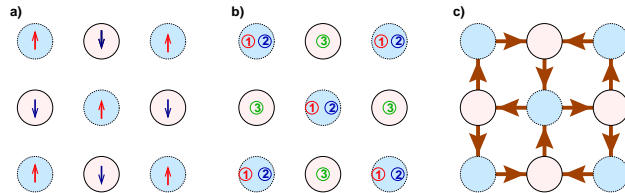


Fig. 4. Types of order in the $U > 0$ fermionic SU(3) Hubbard model. a) AF spin-density wave for $N = 2$. b) Flavor-density wave state for $N=3$. Flavor 1 and 2 prefer one sublattice, flavor 3 the other. c) Staggered flux state for $N > 6$: particle currents are indicated by arrows. Figures taken from [35].

These systems can be used to realize fermionic Hubbard models with $N > 2$ flavors and approximate SU(N) flavor symmetry. In the following we

will discuss the rich physics of these models for finite N , following [35,36]. The Hamiltonian is given by

$$H = -t \sum_{m, \langle ij \rangle} [c_{i,m}^\dagger c_{j,m} + c_{j,m}^\dagger c_{i,m}] + \frac{U}{2} \sum_i n_i^2 \quad (3)$$

where c_{im}^\dagger creates a fermion of flavor $m = 1, \dots, N$ on site i and $n_i = \sum_m n_{i,m}$ is the total number of atoms on site i . Note that the interaction term has local $SU(N)$ invariance while the hopping reduces this to a global one. The values of t and U can be derived from atomic parameters along the lines of section 2.1.

While the large- N limit of this model has been well studied in the context of high- T_c superconductivity [37], few results have been previously obtained for finite N . Consider first the case of repulsive interactions $U > 0$. We have performed a systematic analysis of weak-coupling instabilities using a perturbative functional renormalization group (RG) approach [38]. Although the RG eventually breaks down at strong coupling, it allows to identify the leading instability towards an ordered phase. The analysis performed in [35] focusses on $d = 2$ dimensions.

In Fig. 4 the three relevant types of order at half filling $\langle n_i \rangle = N/2$ are shown. In the spin 1/2 case the system displays staggered antiferromagnetic order, as is well known. For intermediate $N < 6$ the RG yields an instability towards flavor density wave states with ordering wavevector $\mathbf{Q} = (\pi, \pi)$ like in the antiferromagnetic case. This corresponds to a breaking of the $SU(N)$ symmetry, with a degenerate ground state manifold. As N increases, breaking of $SU(N)$ becomes less favorable because the number of Goldstone modes increases. For $N > 6$ the RG indicates a dominant instability of the *staggered flux* type with alternating particle currents around the plaquettes of the 2d lattice (see Fig. 4c).

Let us briefly discuss the temperature scales T_c below which the respective long range orders set in. The critical temperature for flavor density waves at strong coupling scales like t^2/U and can thus be tuned to relatively large values: for $N = 3$ the RG predicts a maximum of $T_c \approx 0.1t$. On the other hand, staggered flux order, like d-wave superconductivity away from half filling, requires significantly lower temperatures, with a typical RG estimate given by $T_c \approx 0.01t$ for $N = 7$. This is about an order of magnitude below the current experimental limit and will require improved cooling techniques.

Next, we focus on the situation with attractive interactions $U < 0$ and $N = 3$ flavors which is relevant for Li^6 . A large recent experimental effort has been devoted to the BEC-BCS crossover in spin-1/2 superfluid fermions [10,11,12,39]. A common feature of these experiments with K^{40} and Li^6 is the use of a Feshbach resonance to generate large attractive interaction. These resonances generally occur only between two hyperfine spin states and thus cannot be used to realize an $SU(3)$ symmetric model. However, as pointed out above, Li^6 has a remarkably large and negative background scattering

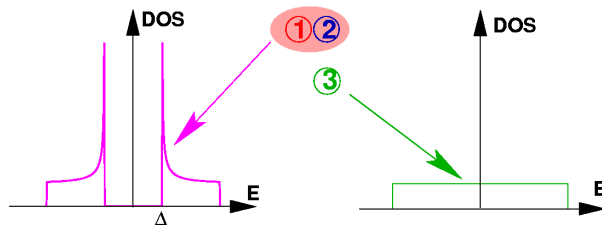


Fig. 5. BCS pairing of 3-flavor fermions with $SU(3)$ symmetry. Note that one flavor remains unpaired, with a normal Fermi surface. Figure taken from [36].

length which in a finite magnetic field is approximately equal for the three spin states with $m_s = 1/2$. In combination with an optical lattice one can thus realize the $SU(N)$ Hubbard model (3) with $U < 0$ and $N = 3$. The possibility of a three-flavor paired state in Li^6 , without consideration of the $SU(3)$ symmetry, has already been pointed out by Leggett [40].

Following the analysis in [36] we now discuss how the spin-1/2 BCS state is generalized to three flavors. We introduce a pairing mean-field and Hamiltonian

$$\Delta_{\alpha\beta} = -\frac{U}{N} \sum_{\mathbf{k}} \langle c_{\mathbf{k}\alpha} c_{-\mathbf{k}\beta} \rangle \quad H_{\text{MF}} = -\frac{1}{2} \sum_{\mathbf{k}, \alpha, \beta} c_{\mathbf{k}\alpha}^\dagger c_{-\mathbf{k}\beta}^\dagger \Delta_{\beta\alpha} + h.c. \quad (4)$$

where $\alpha, \beta = 1, \dots, 3$ are flavor indices and N is the number of lattice sites. We focus on s-wave pairing which is favorable for strong onsite attraction. The Pauli principle then requires antisymmetry $\Delta_{\alpha\beta} = -\Delta_{\beta\alpha}$ in the flavor index. The order parameter can therefore be written as a triplet $\Delta_\alpha = \frac{1}{2} \epsilon_{\alpha\beta\gamma} \langle c_\beta c_\gamma \rangle = (\Delta_{23}, -\Delta_{13}, \Delta_{12})$. From mean-field theory we obtain that all ground states consistent with $\sum_\alpha |\Delta_\alpha|^2 = \Delta_0^2$ are degenerate. This five-dimensional ground-state manifold is consistent with the number of collective modes obtained via Goldstone's theorem.

The remarkable feature of this triplet s-wave state is that superfluid Cooper pairs coexist with a normal Fermi surface (see Fig. 5), i.e. the single-particle spectrum is only partially gapped. This has consequences for the collective modes which we have analyzed within a generalized RPA scheme [36]. They are partially visible in the dynamical structure factor $S(q, \omega)$, which is accessible via Bragg scattering [25]. An example of the calculated density response $\text{Im}\chi^\rho(q, \omega)$ is shown in Fig. 6.

From BCS mean-field theory in two dimensions we find a transition temperature of $T_c = 0.17t$ for typical parameters $n = 3/8$ and $U = -4t$. This amounts to roughly $0.05T_F$ and is within reach of present cooling techniques. Multi-component Fermi systems like Li^6 can thus provide exotic new many-body physics and may even allow quantum simulations of simplified QCD models where only the color degree of freedom is taken into account.

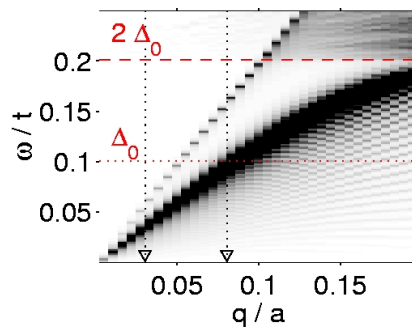


Fig. 6. Density response spectrum $\chi''(q, \omega)$ (equivalent to $S(q, \omega)$) of the 2d fermionic SU(3) Hubbard model at $T = 0.01t$, $U = -4t$ and filling $n \approx 0.55$. The Anderson-Bogoliubov mode, the signature of superfluidity, is clearly visible (thick black line) as well as an additional flavor mode indicating the 3-flavor degeneracy. Figure taken from [36].

4 Disorder and Interaction

So far in this review we have focussed on pure, translationally invariant quantum lattice models. It is indeed one of the main advantages of optical lattices that perfectly disorder-free systems can be realized. On the other hand, effects of impurities and defects are of central importance in solids, where they often compete with the electron-electron interaction [41,42]. It is therefore of great interest to realize in a controlled way disordered cold atom systems where localization effects can be studied.

Experimentally, disordered potentials can be created either with speckle lasers [43] or via quasiperiodic optical lattices [44]. Due to the AC stark effect the atoms experience a spatially fluctuating random potential which is stationary in time. Recently, localization effects have been observed in a BEC subject to a speckle laser field [45].

Here we focus on *fermionic* atoms with two spin states in a three-dimensional optical lattice with an additional random potential. A complete presentation of the results discussed here can be found in [46]. The system is modelled by the Anderson-Hubbard Hamiltonian

$$H_{AH} = -t \sum_{\langle ij \rangle \sigma} c_{i\sigma}^\dagger c_{j\sigma} + \sum_{i\sigma} \epsilon_i n_{i\sigma} + U \sum_i n_{i\uparrow} n_{i\downarrow} - \mu \sum_{i\sigma} n_{i\sigma}, \quad (5)$$

where ϵ_i is a random onsite potential which we assume to be uniformly distributed in the interval $[-\Delta/2, \Delta/2]$. The parameter Δ is a measure of the disorder strength. We focus on the case of half filling $n = 1$ where on average there is one particle per site. The Hamiltonian (5) describes both the interaction-induced Mott transition into a correlated insulator [47,48] as well

as the Anderson localization transition due to coherent backscattering from random impurities [49].

Analyzing the model (5) is a challenging problem. Here we present results obtained within the *Dynamical Mean-Field Theory* (DMFT), a nonperturbative technique where local quantum fluctuations are treated exactly [50,51]. The DMFT has been applied with great success in $d = 3$ spatial dimensions to explain magnetic ordering phenomena and the Mott transition. In the calculation presented here [46] we use a recently developed variant, the *stochastic* DMFT, which is able to describe Anderson localization as well [52,53].

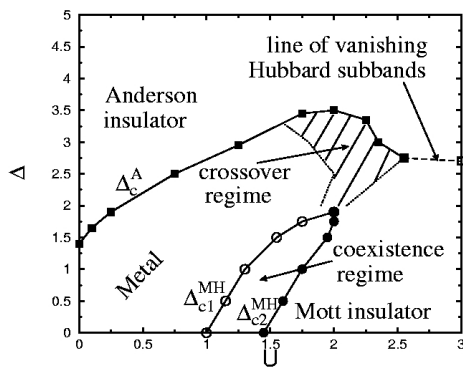


Fig. 7. DMFT ground state phase diagram of the disordered Hubbard model in the nonmagnetic phase at half filling. Figure taken from [46].

Within DMFT, the correlated lattice model is mapped onto a self-consistent Anderson impurity Hamiltonian

$$H_{\text{SIAM}} = \sum_{\sigma} (\epsilon - \mu) c_{\sigma}^{\dagger} c_{\sigma} + U n_{\uparrow} n_{\downarrow} \quad (6)$$

$$+ \sum_{\mathbf{k}\sigma} \left(V_{\mathbf{k}} c_{\sigma}^{\dagger} a_{\mathbf{k}\sigma} + V_{\mathbf{k}}^{*} a_{\mathbf{k}\sigma}^{\dagger} c_{\sigma} \right) + \sum_{\mathbf{k}\sigma} \epsilon_{\mathbf{k}} a_{\mathbf{k}\sigma}^{\dagger} a_{\mathbf{k}\sigma}$$

where a single correlated lattice site now constitutes the impurity with a random onsite energy ϵ , and the fermions $a_{\mathbf{k}\sigma}$ represent a fictitious conduction band with parameters $V_{\mathbf{k}}$ and $\epsilon_{\mathbf{k}}$ which have to be determined self-consistently. The chemical potential $\mu = -U/2$ ensures half filling. This effective single-impurity model is solved using Wilson's numerical renormalization group [54,55,56,57]. Within the stochastic DMFT [53] the self-consistency loop involves a geometric disorder average of the local density of states $\rho_{\text{geom}}(\omega) = \exp[\langle \ln \rho_i(\omega) \rangle]$ which then determines the hybridization function $\eta(\omega) = \sum_{\mathbf{k}} |V_{\mathbf{k}}|^2 / (\omega - \epsilon_{\mathbf{k}})$ for the next iteration. For more details see [46].

The resulting zero temperature phase diagram as a function of disorder Δ and interaction U is shown in Fig. 7. For weak interaction and disorder the atoms are in a Fermi liquid state (“metal”). There are two different metal-insulator transitions: a Mott-Hubbard transition for increasing interaction U , and an Anderson localization transition as a function of Δ . Our results indicate that the two insulating phases are adiabatically connected. Note, however, that in our DMFT calculation we have so far considered only the paramagnetic phase. For non-frustrated lattices (e.g. simple cubic) it is known that an antiferromagnetic instability occurs in the pure Mott state. We are currently analyzing how far this antiferromagnetic phase extends into the disordered Mott-Anderson insulator [58]. Let us briefly comment on the detection of these different phases. Itinerant versus insulating behavior can be identified by a time-flight measurement as in [16]. In the Fermi liquid state, delocalization of fermions across the lattice leads to an interference pattern which vanishes once the atoms become localized. In order to distinguish the antiferromagnetic Mott insulator from the paramagnetic Anderson insulator one could apply spin-resolved Bragg scattering.

Optical lattices are a promising tool to simulate the above phase diagram experimentally since, in contrast to solids, both parameters U and Δ can be tuned arbitrarily. In particular, measurements can be done both in two and three spatial dimensions, possibly detecting qualitatively new physics in $d = 2$ where DMFT is no longer expected to be a good approximation.

5 Summary and Outlook

In this review we have presented some theoretical aspects of strongly correlated atoms in optical lattices. We have shown that these systems can be used to create analogues of well established solid-state quantum phases, but with much higher tunability of the model parameters. More generally, ultracold atoms can be used to perform quantum simulations of solid-state Hamiltonians like the 2d Hubbard model which may be relevant for high-temperature superconductivity. As another example for such a simulation we have discussed interacting fermions with disorder. Within a DMFT calculation we observe remarkable re-entrance into the itinerant phase due to competing Mott- and Anderson-localization. Finally, we have demonstrated that it is possible to use the highly degenerate internal states of cold atoms to create new exotic quantum states which have no analogue in condensed matter physics. Bosons with multiple spin states can be used to create tunable spin hamiltonians. Most prominently, we have discussed a new fermionic SU(3) triplet superfluid state which is a toy model for QCD at weak to intermediate interactions. Experimental realization of these quantum phases is within reach and could significantly increase our understanding of the many-body model systems involved.

6 Acknowledgments

The author would like to thank E. Altman, B. Byczuk, I. Cirac, E. Demler, C. Honerkamp, M.D. Lukin, D. Vollhardt, and P. Zoller for collaborations, and I. Bloch, M. Greiner, M. Zwierlein and W. Ketterle for discussions.

References

1. For a review see special issue of Nature, Vol. **416**, 206 (2002).
2. B. DeMarco and D.S. Jin, Science **285**, 1703 (1999).
3. A.G. Truscott *et al.*, Science **291**, 2570 (2001).
4. F. Schreck *et al.*, Phys. Rev. Lett. **87**, 80403 (2001).
5. Z. Hadzibabic, Phys. Rev. Lett. **88**, 160401 (2002).
6. S. Inouye *et al.*, Nature **392**, 151 (1998).
7. E. Timmermans *et al.*, Phys. Lett. A **285**, 228 (2001).
8. M. Holland *et al.*, Phys. Rev. Lett. **87**, 120406 (2001).
9. Y. Ohashi and A. Griffin, Phys. Rev. A **67**, 033603 (2003).
10. C.A. Regal, M. Greiner, and D.S. Jin, Phys. Rev. Lett. **92**, 040403 (2004).
11. M.W. Zwierlein *et al.*, Phys. Rev. Lett. **92**, 120403 (2004).
12. M. Bartenstein *et al.*, Phys. Rev. Lett. **92**, 120401 (2004).
13. C. Orzel *et al.*, Science **291**, 2386 (2001).
14. M. Greiner *et al.*, Nature (London) **415**, 39 (2002).
15. D. Jaksch *et al.*, Phys. Rev. Lett. **81**, 3108 (1998).
16. M. Köhl *et al.*, preprint cond-mat/0410389.
17. W. Hofstetter *et al.*, Phys. Rev. Lett. **89**, 220407 (2002).
18. M.A. Cazalilla, J. Phys. B: At. Mol. Opt. Phys. **37**, 1 (2004).
19. B. Paredes *et al.*, Nature **429**, 277 (2004).
20. Th. Stöferle *et al.*, Phys. Rev. Lett. **92**, 130403 (2004).
21. C. Kollath *et al.*, PRA **69**, R031601 (2004).
22. C. Kollath *et al.*, preprint cond-mat/0411403.
23. J. Hubbard, Proc. Roy. Soc. London A **276**, 238 (1963).
24. D.J. Scalapino, Physics Reports **250**, 329 (1995).
25. D.M. Stamper-Kurn and W. Ketterle, Les Houches lecture notes 1999 and cond-mat/0005001.
26. R. Feynman, Int. J. Theor. Phys. **21**, 467 (1982).
27. D.M. Stamper-Kurn *et al.*, Phys. Rev. Lett. **80**, 2027 (1998).
28. O. Mandel *et al.*, Phys. Rev. Lett. **91**, 010407 (2003).
29. E. Altman, W. Hofstetter, E. Demler, and M.D. Lukin, New Journal of Physics **5**, 113.1 (2003).
30. L.-M. Duan, E. Demler, and M.D. Lukin, Phys. Rev. Lett. **91**, 090402 (2003).
31. K. Sheshadri *et al.*, Europhys. Lett. **22**, 257 (1993).
32. E. Altman, E. Demler, and M.D. Lukin, Phys. Rev. A **70**, 013603 (2004).
33. C.A. Regal and D.S. Jin, Phys. Rev. Lett. **90**, 230404 (2003).
34. E.R.I. Abraham *et al.*, Phys. Rev. A **55**, R3299 (1997).
35. C. Honerkamp and W. Hofstetter, Phys. Rev. Lett. **92**, 170403 (2004).
36. C. Honerkamp, and W. Hofstetter, Phys. Rev. B **70**, 094521 (2004).
37. J.B. Marston and I. Affleck, Phys. Rev. B **39**, 11538 (1989).
38. C. Honerkamp and M. Salmhofer, Phys. Rev. Lett. **87**, 187004 (2001).

39. M.W. Zwierlein *et al.*, preprint cond-mat/0412675.
40. A. Modawi and A.J. Leggett, *Journal of Low Temp. Phys.* **109**, 625 (1997).
41. P.A. Lee and T.V. Ramakrishnan, *Rev. Mod. Phys.* **57**, 287 (1985).
42. D. Belitz, and T.R. Kirkpatrick, *Rev. Mod. Phys.* **66**, 261 (1994).
43. P. Horak, J.Y. Courtois, and G. Grynberg, *Phys. Rev. A* **58**, 3953 (1998).
44. L. Guidoni *et al.*, *Phys. Rev. Lett.* **79**, 3363 (1997).
45. J.E. Lye *et al.*, preprint cond-mat/0412167.
46. K. Byczuk, W. Hofstetter, and D. Vollhardt, *Phys. Rev. Lett.* **94**, 056404 (2005).
47. N.F. Mott, *Proc. Phys. Soc. A* **62**, 416 (1949).
48. K. Byczuk, W. Hofstetter, and D. Vollhardt, *Phys. Rev. B* **69**, 045112 (2004).
49. P.W. Anderson, *Phys. Rev.* **109**, 1492 (1958).
50. W. Metzner and D. Vollhardt, *Phys. Rev. Lett.* **62**, 324 (1989).
51. A. Georges *et al.*, *Rev. Mod. Phys.* **68**, 13 (1996).
52. V. Dobrosavljević and G. Kotliar, *Phys. Rev. Lett.* **78**, 3943 (1997).
53. V. Dobrosavljević, A.A. Pastor, and B.K. Nikolić, *Europhys. Lett.* **62**, 76 (2003).
54. K.G. Wilson, *Rev. Mod. Phys.* **47**, 773 (1975).
55. T.A. Costi, A.C. Hewson, and V. Zlatić, *J. Phys.: Cond. Mat.* **6**, 2519 (1994).
56. R. Bulla, A.C. Hewson, and Th. Pruschke, *J. Phys.: Condens. Matter* **10**, 8365 (1998).
57. W. Hofstetter, *Phys. Rev. Lett.* **85**, 1508 (2000).
58. K. Byczuk, W. Hofstetter, and D. Vollhardt, in preparation.